Applied Catalysis B: Environmental 331 (2023) 122684

Contents lists available at ScienceDirect

Applied Catalysis B: Environmental

journal homepage: www.elsevier.com/locate/apcatb

Breaking Volmer step limitation on NiO/PtNi heterojunctions via ATO-induced charge injection and interfacial modulation

Yangyang Tan [a], Zeyi Zhang [a], Wei Wu [a], Suhao Chen [a], Wei Chen [a], Niancai Cheng [a,b,*]

[a] College of Materials Science and Engineering, Fuzhou University, Fuzhou 350108 China
[b] Key Laboratory of Fuel Cell Technology of Guangdong Province, Guangzhou, Guangdong 510641, China

ARTICLE INFO

Keywords:
NiO-PtNi Heterostructures
Interface component regulation
Alkaline HER

ABSTRACT

Driven by the persisting poor understanding of the slow kinetics of hydrogen evolution (HER) on Pt-based alloys in alkaline media, it is necessary and challenging to explore the clear relationship between heterogeneous interface components and activity. Herein, we develop an exquisite triphasic interfacial structure featuring the Sb-doped SnO_2 (ATO)-supported NiO/PtNi heterojunction with controllable heterogeneous interface. The strong electron-donating effect of the ATO carrier and the electronic coupling between PtNi and appropriate NiO components effectively optimize the adsorption of H_2O^* and dissociation of H*, especially the adsorption-dissociation of H_2O on the NiO site (Volmer step), thus accelerating the overall alkaline HER kinetics. The resulting catalyst delivers high alkaline HER performances with a low Tafel slope (only 25.5 mV dec^{-1}) and an ultra-long stability of 140 h operation. Our findings provide new insights into breaking the water dissociation limit of Pt-based catalysts by rational design of heterogeneous interfaces.

1. Introduction

Water-alkali electrolyzers has the advantages of simplicity, high purity product and robustness of facilities, and has been regarded as an advanced sustainable energy storage technology approach to alleviate the dependence on fossil fuels [1–3]. Despite decades of industrialization, the catalytic efficiency of cathodic-alkaline hydrogen evolution reaction (HER) is still much lower than under acidic media mainly due to the higher initial water dissociation energy barrier (Volmer step : $H_2O + * + e^- \leftrightarrows H^* + OH^-$) [4–7]. Theoretically, an efficient alkaline HER catalyst should have a low water dissociation barrier and appropriate (Sabatier principle) H* adsorption energies [8,9]. Up to now, platinum (Pt) catalysts with suitable H* binding energy are still regarded as the best HER catalysts, but the inferior ability to resolve OH-H bonds limits its overall alkaline HER activity [10–14]. Therefore, simultaneously achieving rapid water dissociation and subsequently H* adsorption/-conversion processes of Pt-based catalysts is crucial but challenging for realizing the efficient industrialization of alkaline hydrogen production.

Heterogeneous interfacial engineering consisting of dual active sites of Pt and water dissociation promoters, such as transition-metal oxides/hydroxides/sulfides/ phosphides , allowing separate reaction steps to occur on adjacent sites [15–21], has been demonstrated as an effective strategy to enhance the alkaline HER activity of Pt-based catalysts. Yet, due to the Schottky barrier formed at the Pt/metal compound interface by the work function difference, an additional overpotential is often required to overcome built-in voltage, which weakens the multicomponent advantage and resulting in suboptimal alkaline HER activity [22,23]. In this regard, previous studies have proved that bimetallic nanocrystals with high compositional segregation can be developed into heterostructures with close interfaces due to the inherent differences in the chemical reactivity of the metal components [24–26]. For instance, Huang et al. [27] have synthesized a Pt_3Ni_2 NWs-S/C catalyst with Pt_3Ni_2-NiS heterogeneous interface by simple sulfuring highly composition-segregated PtNi nanowires, which exhibits the high HER performance in 1 M KOH solution. Huang et al. [28]synthesized a PtNi-O catalyst with enriched NiO/PtNi interface by heat-treating octahedral PtNi/C in an air atmosphere, achieving high HER activity and stability. Despite extensive efforts, the Tafel slopes of alkaline HER of most reported Pt-based dual-site catalysts reported above are still higher than 30 mV dec^{-1}, indicating that these catalysts have not yet broken the limit of the Volmer step. In addition, the above-mentioned efforts are mainly focused on morphological tuning to optimize the dual-site functionality, rather than optimizing the electronic structure of the Pt-based dual-site catalysts to enhance the inherent adsorption free energy for

* Corresponding author at: College of Materials Science and Engineering, Fuzhou University, Fuzhou 350108 China.
E-mail address: niancaicheng@fzu.edu.cn (N. Cheng).

https://doi.org/10.1016/j.apcatb.2023.122684
Received 9 November 2022; Received in revised form 23 February 2023; Accepted 22 March 2023
Available online 23 March 2023

H-intermediates, thus leaving plenty of room for further improving of the HER performance.

Sb-doped SnO_2 (ATO), an n-type conductive direct bandgap semiconductor, is considered a good carrier material due to its metal-like properties as well as its high corrosion resistance in acidic and alkaline environments and high electronic conductivity [29,30]. Studies have shown that ATO can induce electronic effects on Pt catalysts, thereby exhibiting stronger activity and persistence in the formic acid oxidation reaction [31,32]. In this context, using ATO as a conductive substrate in combination with a highly composition segregated PtM alloy to construct a novel heterogeneous interfacial structure with strong interfacial electron coupling, which is expected to break the limitation of water dissociation and thus enhance the alkaline HER activity of Pt-based catalysts.

Based on the above assumption, density functional theory (DFT) calculations were first performed to confirm that the electron-donating effect of ATO can enrich the charge distribution of Pt and Ni atoms leading to negative shift of their d-orbital, in which the activation energy of H_2O at the NiO site is optimized to enhance the Volmer step activity, while the adsorption free energy of H*is reduced at the Pt site in PtNi to promote the following Tafel step. Guided by this result, we have constructed a triphasic interfacial structure electrocatalyst featuring the ATO-supported PtNi/NiO heterojunction via induced in-situ Ni diffusion from PtNi to surface to form NiO. The introduction of ATO carriers reduces the activated electronic states of Pt and Ni atoms at the Fermi energy level, which facilitates the desorption behavior of intermediate states on them. In addition, the strong electronic coupling of the dual-active site between the precisely tuned NiO and the adjacent PtNi alloy further provides optimized interaction energies for the reaction intermediates (H_2O* and H*), thus allowing the catalyst to break the limitation on H_2O dissociation (Volmer step) and enabling a fast HER kinetics in alkaline media. As a result, the optimized NiO-PtNi/ATO catalyst displays excellent alkaline HER activity with Tafel slope of only 25.5 mV dec^{-1}, the minimum overpotential (23.1 mV) at 10 $mA{\cdot}cm^{-2}$, the highest mass activity of 8.4 A mg_{Pt}^{-1} at 70 mV and the ultra-long operation time (140 h), far exceeds the commercial Pt/C catalyst and most recently reported Pt-based catalysts.

2. Experimental section

2.1. Catalysts synthesis

ATO, PtNi/ATO and NiO-PtNi/ATO: The preparation of ATO was same to the previous research.[33] In a typical preparation of PtNi/ATO, the obtained ATO (100 mg), Ni $(NO_3)_2{\cdot}6\ H_2O$ (50 mg), $H_2PtCl_6{\cdot}6H_2O$ (89 mg) and ethylene glycol (80 ml) were put into a three-neck flask with a PtNi loading of 10 wt% and a Pt:Ni theoretical atomic ratio of 1, and ultrasonically mixed well. Then the flask was placed in an oil bath under N_2 atmosphere for 2 h at 160 ℃ condensing and refluxing, and removed and cooled to room temperature. After centrifugation, the sample was washed three times with deionized water by filtration. Finally, the samples were freeze-dried, collected and named as PtNi/ATO. The obtained PtNi/ATO (50 mg) was placed in the middle of a quartz boat and placed in a tube furnace under N_2-saturated atmosphere at 200, 300, 400 and 600 °C for 2 h to obtain the samples (Ni-PtNi/ATO-x, x represents the heat treatment temperature). Finally, Ni-PtNi/ATO-x was oxidized under air atmosphere at 200 °C for 1 h to obtain NiO-PtNi/ATO-x series samples, of which NiO-PtNi/ATO-200 was also named as NiO-PtNi/ATO.

Pt/ATO, Pt/ATO-200, PtNi/C and NiO-PtNi/C: Pt/ATO and Pt/ATO-200 were prepared as control samples using the same methods as for PtNi/ATO and NiO-PtNi/ATO except in the absence of Ni $(NO_3)_2{\cdot}6\ H_2O$. PtNi/C, PtNi/C-200 and PtNi/C-400 were prepared as control samples using the same methods as for PtNi/ATO and NiO-PtNi/ATO except in the substitute XC-72 carbon for ATO and thermal treatment temperature.

Acid-NiO-PtNi/ATO: The NiO-PtNi/ATO sample (30 mg) was placed in a 50 ml beaker containing 30 ml of 0.5 M H_2SO_4 solution, and then stirred for 12 h. Finally, the sample was rinsed several times with ultrapure water and freeze-dried overnight to obtain Acid- NiO-PtNi/ATO samples.

2.2. Materials characterization

The morphology of the samples were characterized by aberration correction field emission transmission electron microscope (Titan G2 60–300 with image corrector). X-ray powder diffraction (XRD) was measured on Rigaku ULTIMA III. X-ray photoelectron spectroscopy (XPS) characterization was obtained on VG ESCALAB 250 (corrected by referencing the energies of the C 1 s peak at 284.6 eV). The Pt content of catalysts were tested through inductively coupled plasma atomic emission spectroscopy (ICP-AES).

2.3. Electrochemical measurement

A three-electrode system in alkaline medium (1 M KOH) was used to evaluate the HER performance of the catalyst by means of an electrochemical workstation (CHI 760E), where the prepared catalysts were used as working electrodes, and graphite rods and Ag/AgCl electrodes were used as counter and reference electrodes (vs. RHE), respectively. The prepared catalyst (2 mg) and XC-72 carbon (0.5 mg) were dispersed uniformly in 1 ml of a water/isopropanol (1:1) mixture containing 10 μL of 5% Nafion. Then, take 10 μL of catalyst ink to form a uniform film with a mass loading to 0.127 mg cm^{-2} on a glassy carbon electrode (diameter: 5 mm).

Cyclic voltammetry (CV) curves were scanned in Ar-saturated 1 M KOH solution at a scan rate of 50 mV s^{-1} in the range of 0.05–1.2 V, and then the chronopotentiometric curves were executed at 10 mA cm^{-2}. The 95% iR-compensated (0.1 ∼ −0.2 V resistance) linear scanning voltammetry curves (LSV) were recorded at a scan rate of 5 mV s^{-1}(Details in Supporting Information).

3. Results and discussion

3.1. Theory prediction

In alkaline media, the adsorption-dissociation step of H_2O molecules and moderate M-H_{ad} binding energy are considered as two key indicators reflecting the intrinsic catalytic activity of HER catalyst. Theoretically, since the catalytic intermediate is strongly dependent on the charge distribution at the catalyst surface, specialized charge tuning might allow the NiO-PtNi heterojunction to achieve an attractive HER activity. Thus, prior to synthesizing the NiO-PtNi/ATO electrocatalysts, we first carried out DFT calculations to investigate the feasibility of ATO carrier to improve HER performance of NiO-PtNi heterojunction. As shown in Fig. S1, NiO-PtNi nanoparticles were placed on ATO (Sb substitute Sn atoms) and graphene carbon layers, respectively, to explore the carrier effects on the electronic structure. The charge density difference analysis revealed the obvious charge redistribution at the interface between ATO carriers and NiO-PtNi compared to C carriers (Fig. 1a and Fig. S1), indicating ATO can induce more electron transfer at the heterogeneous interface. The density of state projection (PDOS) (Fig. 1b) further shows that the d-band centers of Pt (−1.94 eV) and Ni (−1.67 eV) in NiO-PtNi/ATO are more away from the Fermi level (E_f) than that in NiO-PtNi/C (Pt: −1.76 eV; Ni: −1.51 eV), suggesting the Pt and Ni atoms in NiO-PtNi/ATO obtain electrons from ATO. According to the d-band center theory, the downward shift of E_d leads to the delocalization of the antibonding unoccupied orbital [34–36], favoring the activation and cleavage of HO-H and thus promoting water dissociation. To further verify the above statement, DFT calculation of Gibbs free energy for HER was performed. In this part, due to the excellent hydrophilicity of NiO [16,37,38] and the high H* reduction-conversion

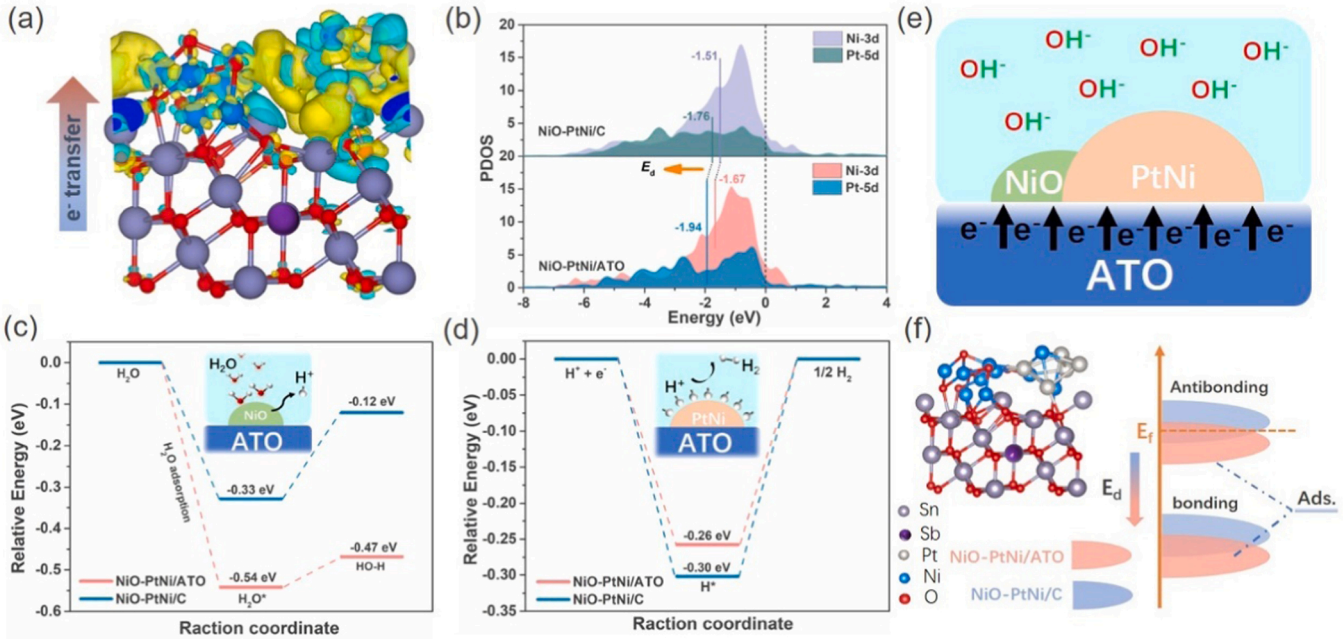

Fig. 1. Theoretical design of the catalyst. (a) Graphical representations of the electron transfer between NiO-PtNi nanoparticles and the support (ATO). (b) Charge density redistribution of the heterostructure constructed by joining an ATO and NiO-PtNi nanoparticles. (c) The partial density of states (pDOS) and d-band center of Ni and Pt atom, and corresponding energy differences for (d) the water dissociation process and (e) the diagram of ΔG_H for NiO-PtNi/ATO and NiO-PtNi/C. (f) Schematic illustration of bond formation between the catalyst surface and the adsorbates (Ads.).

activity of PtNi [4,36,39], NiO and PtNi in NiO-PtNi/ATO model were selected as the active sites for H_2O adsorption-dissociation (Volmer step) and the subsequent conversion of H* to H_2, respectively. In Fig. 1c, we found that NiO-PtNi/ATO exhibited more spontaneous H_2O activation ability and lower H_2O dissociation barrier (0.07 eV) under the assistance of ATO carrier compared with NiO-PtNi/C systems, confirming the promotion effect of ATO carrier for the H_2O dissociation of Volmer step. Similarly, the subsequent H* adsorption barrier at the PtNi site was also reduced by 0.04 eV (Fig. 1d), further revealing the positive role of ATO carrier in enhancing H* reducing activity in alkaline media. These results suggest that the introduction of ATO carriers as electron donors provides a new opportunity for the NiO-PtNi heterojunction to accelerate H_2O dissociation and H* evolution in alkaline media. Therefore, as shown in Fig. 1e, interface engineering by loading NiO-PtNi on ATO is proposed to construct a novel alkaline HER electrocatalyst. In this composite interface, the electronic structure and electrocatalytic processes of NiO-PtNi is regulated by ATO substrate. The heterogeneous catalysis can be considered as the coupling between the adsorption valence state and the transition metal d state, separating to form the bonding and antibonding states [34,40]. The decrease in the E_d level indicates that the antibonding energy state is filled with more electrons, leading to a weaker interaction between the adsorbent and the surface [41]. These studies provide intrinsic elucidation that charge modulation by ATO can further optimize the active electronic states of Ni and Pt atoms near the Fermi level, leading to a downward shift of their d-band center (Fig. 1f), favoring the desorption of H_2O* and H* at the NiO and PtNi surfaces, respectively, thus accelerating the overall alkaline HER dynamics. In summary, we predict that the electron-donating effect of ATO will greatly boost the alkaline HER performance of NiO-PtNi by tuning the d-band centers of Pt and Ni atoms to facilitate the activation-dissociation of H_2O and subsequent H* adsorption-conversion processes.

3.2. Characterization of electrocatalyst

To verify the DFT prediction, experiments were performed to synthesize the NiO-PtNi/ATO catalyst, the formation process shown in Fig. 2a. First, ATO [32] was used as a carrier to support PtNi alloy nanoparticles through an improved ethylene glycol (EG) reduction method. The obtained PtNi/ATO migrated part of the Ni atoms in the PtNi alloy to the surface due to the inherent compositional segregation of different metals[25,26,42], forming a Ni-PtNi structure by in situ calcination at 200 °C under N_2 atmosphere. Finally, the Ni elements on the Ni-PtNi surface were oxidized in air at 200 °C to form a close-contact and unique NiO-PtNi heterostructure (NiO-PtNi/ATO). As shown in Fig. S2, the prepared pure ATO material was formed by aggregated nanoparticles with a diameter of 5–10 nm. The high-resolution TEM images in Fig. 2b and c clearly shows that in addition to the (110) crystal plane of SnO_2 (d=0.336 nm), the tightly connected lattice fringes with lattice spacing of 0.147 nm and 0.218 nm are observed, which belong to the (220) crystal plane of NiO (Fig. S3) and the (111) crystal plane of PtNi, respectively [37,39]. The formation of NiO results from the oxidation of exposed Ni atoms on the surface of Ni-PtNi during annealing in air [43,44]. The well-defined triphase of NiO and the neighboring lattice of PtNi are coated on the ATO lattice and constructed through the atomic-scale interface. The HAADF-STEM and EDS elemental mapping in Fig. 2d confirm the uniform presence of Pt, Ni, O, Sn and Sb elements on the NiO-PtNi/ATO electrocatalyst. In order to eliminate the influence of ATO carrier on Ni migration, we prepared PtNi/C catalyst with XC-72 carbon instead of ATO in the same way. The XRD pattern of Fig. 2e shows that, in addition to ATO (SnO_2 no. 41–1445), the PtNi diffraction peak of PtNi/ATO is around 42°, and the shoulder peak is between 40.5° and 43.5°, indicating Ni atoms enter the Pt lattice to form PtNi alloy on the surface of ATO [36,45]. The detailed elemental contents are presented in Table S1 by inductively coupled plasma atomic emission spectroscopy (ICP-AES) analysis. After further oxidation at 200 ℃, the characteristic peak of PtNi alloy is significantly negatively shifted to a low angle (Pt, (200) planes), indicating part Ni atoms are separated and migrated from PtNi to the surface to form NiO during heat treatment [46]. The similar results of the XRD spectrum in Fig. S4 indicate that the PtNi alloy restructuring phenomenon is widespread. Furthermore, the XRD pattern in Fig. S5 shows that the diffraction peak of Pt/ATO does not shift after heat treatment, indicating the unique NiO-PtNi structure originates from the in-situ diffusion of Ni

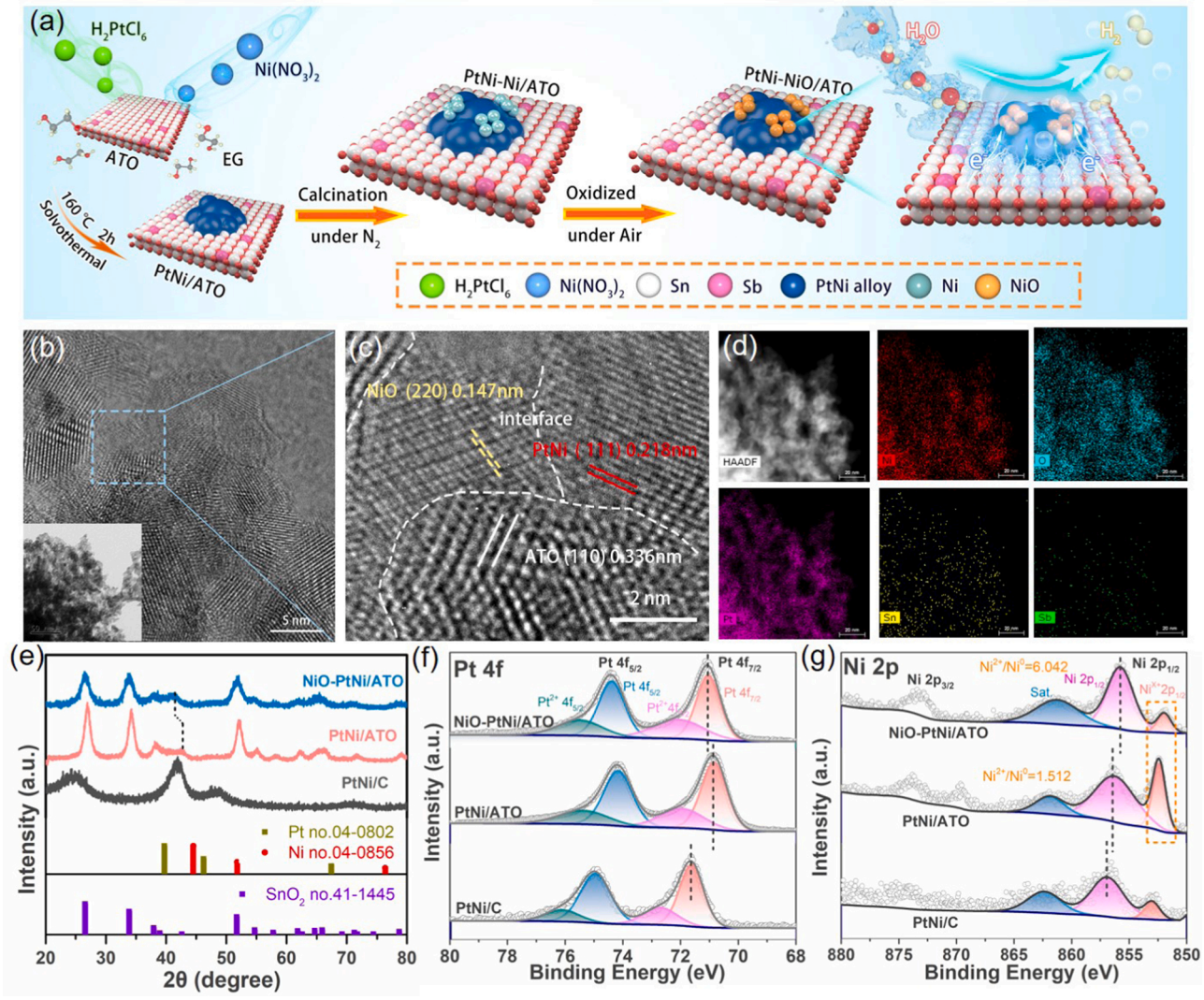

Fig. 2. (a) Schematic illustration of the synthesis of the ATO supported NiO-PtNi heterostructures. (b) HR-TEM image (inset in (b) is the TEM), and (c) magnified regions in NiO-PtNi/ATO. (d) HAADF-STEM and EDS elemental mapping images of NiO-PtNi/ATO. (b) XRD patterns and HR-XPS spectra of (f) Pt 4f and (g) Ni 2p for PtNi/C, PtNi/ATO and NiO-PtNi/ATO.

atoms in the PtNi alloy, independent of the Supporting Material. The above results reveal that the phase transformation of PtNi alloy can be realized by simple secondary heat treatment in N_2 and air, respectively, forming a unique compact NiO-PtNi heterostructure. The electronic state evolution of Pt and Ni elements in C, ATO supports and after oxidation are further explored by X-Ray photoelectron spectroscopy (XPS). The peaks of Pt 4 f, Sn 3d, O 1 s, Sb 3d and Ni 2p can be observed in the XPS survey spectrum (Fig. S6). As shown in Figs. 2f and g, the Pt 4f and Ni2p spectrum of PtNi/ATO are negatively shifted by 0.78 eV and 0.49 eV, respectively, compared to the XC-72 carbon-supported PtNi alloy catalyst (PtNi/C), confirming the strong metal-support interaction between ATO and PtNi alloy allows electron transfer from ATO to Pt and Ni atoms [13,47,48], which matches the DFT results. In addition, the Pt 4f of Pt/ATO without Ni in Fig. S7 also has a significant negative shift compared with the Pt/C catalyst, which further confirms the above conclusion. And after heat treatment, the Pt 4f peak of PtNi/ATO was positively shifted by 0.19 eV while the Ni 2p peak was negatively shifted by 0.67 eV, indicating the electronic coupling between the formed NiO and PtNi by charge transfer from PtNi alloy to NiO [49,50]. Similar results can be observed in XPS spectra of the Pt 4f and Ni 2p of NiO-PtNi/ATO and NiO-PtNi/C (Fig. S8). In addition, a significant increase in the Ni^{2+}/Ni^0 ratio (1.512–6.042) after heat treatment can be observed in Fig. 2g (yellow circle), further verifying that Ni^0 precipitates from the PtNi alloy to form high-valent nickel oxides during the heat treatment [45,51]. These results indicate that the strong electron donating ability of ATO supports increases the charge density of Pt and Ni atoms, and the formation of NiO-PtNi heterojunction helps to further improve the adsorption-dissociation behavior of H_2O molecules, which is expected to break the restriction of HER activity of Pt-based catalysts in alkaline media.

3.3. *Electrocatalytic properties*

To verify the role of ATO support as an electron donor for boosting intrinsic activity, the HER performance of these catalysts was evaluated using the conventional three-electrode configuration in Ar-saturated 1.0 M KOH electrolyte. As shown in Fig. 3a, the NiO-PtNi/ATO shows the highest HER performance among all catalysts, with η_{10} of only 23.1 mV, significantly superior to the PtNi/ATO, PtNi/C and commercial Pt/C catalyst (Fig. 3b). Moreover, the mass activity of NiO-PtNi/ATO normalized loaded Pt mass (6.81 wt%, ICP-OES) at an overpotential of 70 mV is 8.4 A $mg_{Pt^{-1}}$, which is 2.3, 2.5 and 20.0 times higher than that of PtNi/ATO (3.7 A $mg_{Pt^{-1}}$), PtNi/C (3.3 A $mg_{Pt^{-1}}$) and commercial Pt/C catalysts (0.42 A $mg_{Pt^{-1}}$), respectively. These results

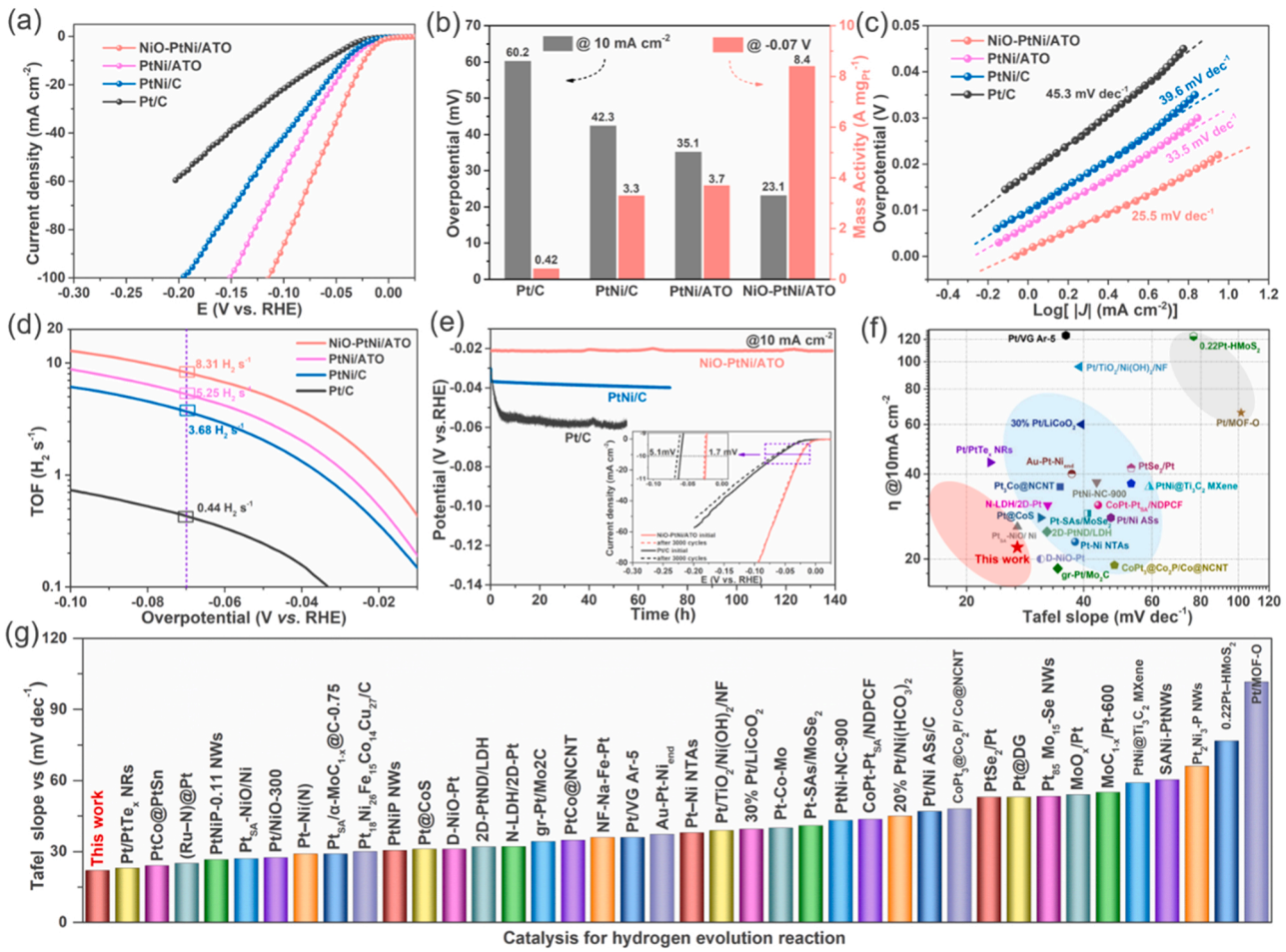

Fig. 3. (a) LSV curves, (b)the overpotential and mass activity, (c) the Tafel plots and (d) corresponding TOF of NiO-PtNi/ATO, PtNi/ATO, PtNi/C and 30% commercial Pt/C, measured in 1 M KOH aqueous solution. (e) Chronopotentiometric curves of NiO-PtNi/ATO, PtNi/C and 30% commercial Pt/C at current densities of 10 mA cm^{-2} (The inset is LSV curves of NiO-PtNi/ATO and commercial Pt/C before and after 3000 cycles). Comparison of (f) η10 values and (g) the Tafel slope for NiO-PtNi/ATO with reported Pt-based catalysts in the last three years, originating from Table S3.

suggest that the intrinsic HER activity of NiO-PtNi was improved by the electron-donating effect of. ATO carrier. In addition, the overpotential of both Pt/ATO-200 (46.3 mV) and NiO-PtNi/C (36.5 mV) at 10 mA cm^{-2} was higher than that of the NiO-PtNi/ATO catalysts further supported this conclusion (Fig. S9). Notably, the significantly optimized polarization profile of PtNi/ATO after heat treatment suggests that the generation of NiO to construct the NiO-PtNi heterostructure also plays a key role in enhancing the alkaline HER activity of NiO-PtNi/ATO. The alkaline HER kinetic behavior of the above electrocatalyst was further investigated by the Tafel slope (Fig. 3c). NiO-PtNi/ATO displays a small Tafel slope of 25.5 mV dec^{-1}, much lower than that of PtNi/ATO (33.5 mV dec^{-1}), PtNi/C (39.6 mV dec^{-1}) and Pt/C (45.3 mV dec^{-1}), indicating that NiO-PtNi/ATO follows a typical Volmer-Tafel HER pathway [52–54]. Notably, most of the reported Pt-based catalysts have Tafel slopes greater than 30 mV dec^{-1}, suggesting that the reaction kinetics are partially controlled by the Volmer-step. Here, the Tafel slope values of NiO-PtNi/ATO indicate that the rate-determining step of the catalyst is H_2 desorption (Tafel step) rather than H_2O dissociation (Volmer step) [4,16,52], thus breaking the limitation of the Volmer step under alkaline HER and balancing the intermediates of the two steps with close to optimized binding energies. In order to reveal the inner activity of per-active site, we further studied the turnover frequency (TOF) values of NiO-PtNi/ATO, PtNi/ATO, PtNi/C and commercial Pt/C calculated based on ICP-AES (Fig. 3**d**). The TOF values of NiO-PtNi/ATO catalyst in the potentiometric region (8.31 s^{-1} at an overpotential of 70 mV) were 1.58, 2.26 and 18.89 times higher than those of PtNi/ATO (5.25 s^{-1}), PtNi/C (3.68 s^{-1}) and Pt/C (0.44 s^{-1}), respectively, further demonstrating that the ATO carrier and NiO-PtNi heterostructures contribute significantly to enhance the intrinsic HER activity of the catalysts. To evaluate the electrochemical active area (ECSA) of the electrocatalysts, we tested the double-layer capacitance (Cdl) of different catalysts in the non-Faraday region [55–57]. As shown in Fig. S10, NiO-PtNi/ATO has a higher Cdl value (41.7 mF cm^{-2}) than PtNi/ATO (31.4 mF cm^{-2}) and PtNi/C (26.1 mF cm^{-2}), indicating that NiO-PtNi/ATO has a higher ECSA. In particular, the current densities of NiO-PtNi/ATO, PtNi/ATO and PtNi/C were normalized to ECSA (Fig. S11), further indicating that NiO-PtNi/ATO has the highest intrinsic activity. HER catalytic stability is another key indicator for practical applications. Fig. 3e shows that the NiO-PtNi/ATO electrode decays almost negligibly during 140 h chronopotentiometry, far superior to PtNi/C and commercial Pt/C catalysts, which should benefit from the charge optimization of the NiO-PtNi active site by the strong electron-donating effect of the ATO carrier. In addition, NiO-PtNi/ATO has almost no potential shift after 3000 cycles test (Δ*E* only 1.7 mV), significantly better than the commercial Pt/C catalyst and exhibits excellent alkaline catalytic stability. Furthermore, NiO-PtNi/ATO showed little change in structure and surface composition after stability testing (Fig. S12), further demonstrating its excellent structural and catalytic stability. Comparing the actual H_2 amount with the theoretical H_2 amount at different reaction times (Fig. S13), the results reveal that the Faraday efficiency (FE) of NiO-PtNi/ATO is 97.6%, indicating that most of the provided electrical energy is used to generate H_2 during the

water splitting process. When comparing the Tafel slope and η10 with the data reported in the literature, we can find that the performance of NiO-PtNi/ATO is one of the most advanced catalysts (Fig. 3f). Furthermore, a comparison of the Tafel slope of NiO-PtNi/ATO and other recently reported Pt-based HER electrocatalysts further reveals the excellent HER reactivity in alkaline media and the advanced nature of constructing NiO-PtNi heterojunctions on ATO carriers (Fig. 3g and Table S3).

3.4. Mechanism discussion

Given the strong effect of NiO component on enhancing the intrinsic HER activity of NiO-PtNi/ATO, we modulated the NiO content by oxidizing PtNi/ATO at different temperatures to reveal the fundamental role of the NiO component. As shown in Fig. 4a, b, the alkaline HER performance of series NiO-PtNi/ATO catalysts showed a trend of increasing and then decreasing in the range of 0–600 °C (Fig. 4c), in which the samples obtained at 200 °C (NiO-PtNi/ATO-200, i.e., NiO-PtNi/ATO) had the highest HER performance. The XRD spectrum (Fig. 4d) shows a gradual negative shift of the characteristic peaks of the PtNi alloy to lower angles (the (200) crystal plane of Pt) with increasing oxidation temperature, increasing the heat treatment temperature causes more Ni atoms to separate from PtNi and migrate to the surface to form NiO, thus achieving the modulation of the NiO component. In addition, the XPS patterns of Pt 4f (Fig. 4e) and Ni 2p (Fig. 4f) showed a positive shift of the Pt 4f peak while a negative shift of the Ni 2p peak with increasing oxidation temperature, which further confirmed that the generation of more NiO led to a more pronounced charge transfer from PtNi to NiO [11,16,58]. The gradually increasing Ni^{2+}/Ni^{0} ratio in Fig. 4f further confirmed this conclusion. The detailed data is summarized in Table S2. These results indicate that precise regulation of the NiO composition can optimize the charge distribution of the NiO/PtNi heterostructure, thereby balancing the water dissociation step and subsequent H* adsorption behavior, and cooperates with the ATO carrier to maximize improving its alkaline HER activity. In addition, as shown in Fig. S14, NiO-PtNi/ATO-400 shows lower hydrogen region area, higher underpotential deposition (H_{upd}) of hydrogen and higher Ni^{2+}/Ni^{3+} redox peak area than NiO-PtNi/ATO-200, these results indicate that the decreased HER activity of NiO-PtNi/ATO samples obtained at higher oxidation temperature may be due to the fact that the Pt site on the surface of ATO is almost covered by excessive NiO, resulting in decreased H^{+} adsorption energy and low catalytic efficiency.

In order to clarify the key role of nickel oxide, we removed the nickel oxide on the surface of NiO-PtNi/ATO in 0.5MH_2SO_4 solution, and then investigated the HER electrocatalysis of the Acid-NiO-PtNi/ATO catalyst (see supporting information for details). As shown in Fig. S15a, **b**, **c**, the recovered low Ni^{2+}/Ni^{0} ratio in Ni 2p spectrum and the disappearance of the redox peak of Ni^{2+}/Ni^{3+} (1.32 V/1.39 V) in the CV curve together with the negative shift of Pt in Pt 4 f spectrum confirmed the successful removal of NiO species on the surface of the PtNi alloy of the Acid-NiO-PtNi/ATO. Compared with NiO-PtNi/ATO, the significantly reduced mass activity (6.2 A mg_{Pt}^{-1}) and increased Tafel slope (33.8 mV dec^{-1}, higher than 30 mV dec^{-1}) of Acid-NiO-PtNi/ATO (Fig. S15c, d, e) clearly demonstrating the surface NiO-modified PtNi alloy heterostructure plays an indispensable role to accelerating the Volmer step and improving the overall alkaline HER kinetics.

Driven by the large difference in alkaline HER activity between NiO-PtNi/ATO and NiO-PtNi/ATO-300, we used DFT calculations to decipher the modulation essence of NiO composition regulation on water dissociation and subsequent reaction mechanism. As shown in Fig. S16, taking the exposed Pt (111) and pure PtNi model as a reference, NiO-PtNi heterostructure model with a small amount of NiO nanoclusters on the PtNi surface and NiO(rich)-PtNi model with a layer of NiO on the PtNi surface were constructed, respectively. As shown in Fig. 5a and b, the construction of the NiO/PtNi contact resulted in a redistribution of the electronic structure at the interface of the heterostructure due to the different electronegativity of the atoms (3.44 for the O atom, 1.91 for the Ni atom, and 2.28 for the Pt atom), that is, the charge changes from Ni atoms and Pt atoms are transferred to adjacent O atoms. In particular, the appropriate NiO content in PtNi-NiO enables the simultaneous charge polarization of the exposed Pt and NiO sites, thereby enhancing the binding strength to OH* and H*, respectively. In addition, the PDOS

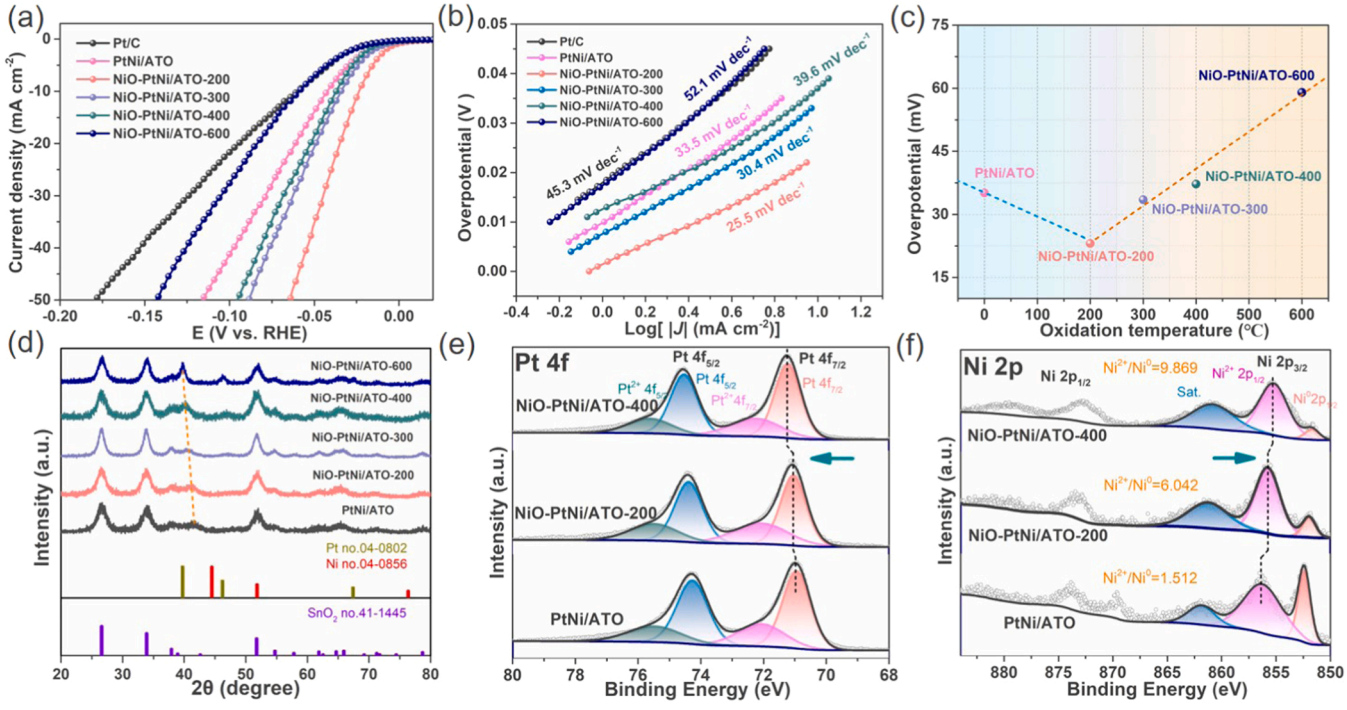

Fig. 4. (a) HER polarization curves, (b) Corresponding Tafel slopes and (c) The relationship between oxidation temperatures and overpotential obtained from experiments for different NiO-PtNi/ATO catalysts. (d) XRD patterns of catalysts obtained at different oxidation temperatures. (e) XPS survey spectra in Pt 4 f and (f) Ni 2p of PtNi/ATO, NiO-PtNi/ATO-200 and NiO-PtNi/ATO-400.

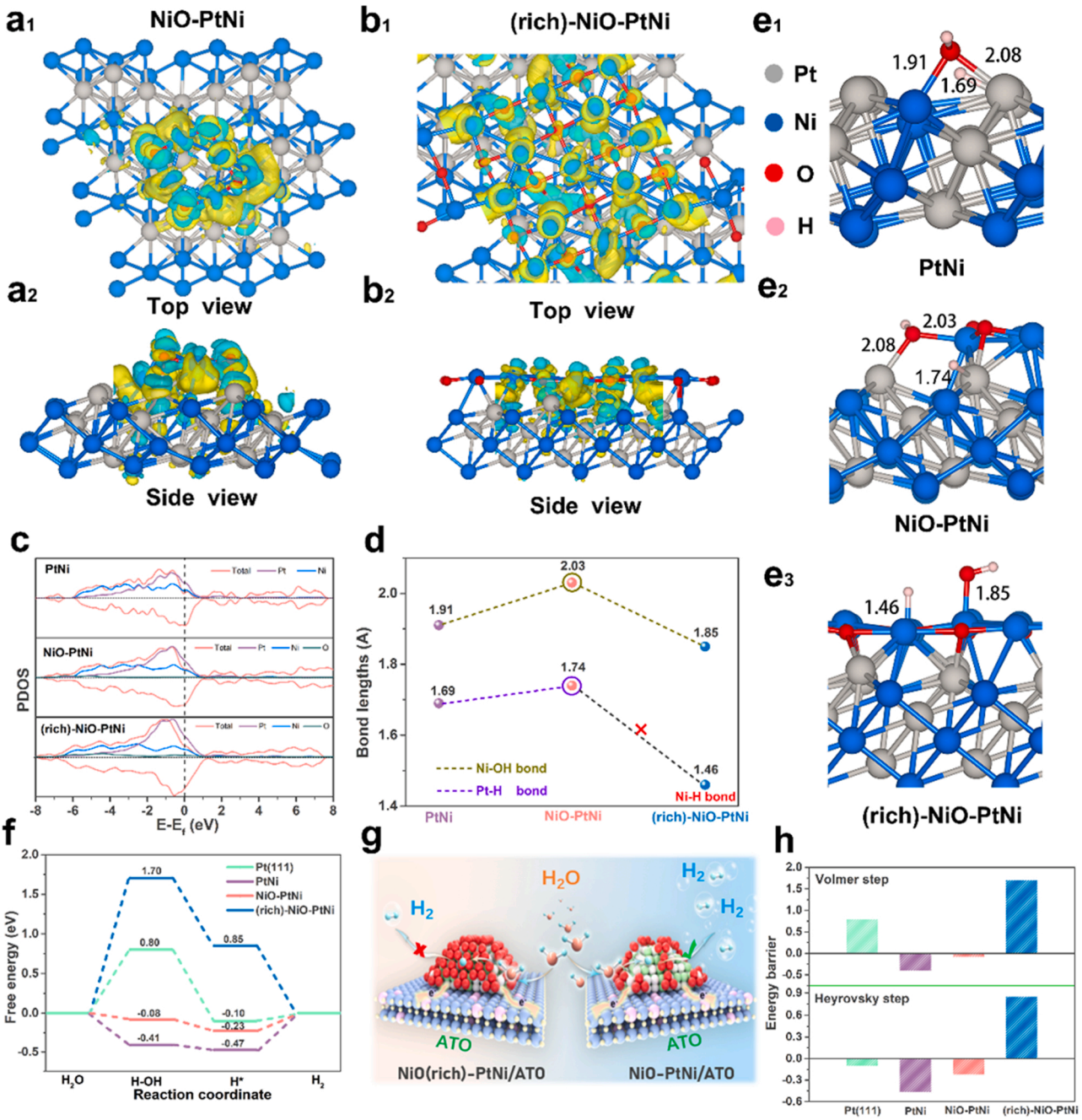

Fig. 5. The electron density difference of (a_1, a_2) NiO-PtNi and (b_1, b_2) (rich)NiO-PtNi (Top and side view; the blue and yellow isosurfaces show the electron losing and gaining, respectively). (c) The projected density of states (PDOS) of Pt on PtNi, NiO-PtNi and (rich)NiO-PtNi. (d-e) Calculated activated Ni-OH and Pt-H bond lengths on PtNi, PtNi-NiO and PtNi-(rich)NiO. (f) The free energy diagram for alkaline HER on Pt (111), PtNi, PtNi-NiO, and PtNi-(rich)NiO. (g) Schematic illustration for the differences of NiO-PtNi and (rich)NiO-PtNi during the alkaline HER. (h) Calculated OH-binding energies (ΔE_{OH}) and H binding energies (ΔE_H) for Pt (111), PtNi, PtNi-NiO, and PtNi-(rich)NiO.

of Pt, Ni atoms in PtNi, NiO-PtNi and (rich)NiO-PtNi were investigated (see Fig. 5**c**). By comparing the electronic states near the Fermi level, the highest electron localization in (rich)NiO-PtNi was observed in the three models, indicating that more electron transfer occurs at the interface in (rich)NiO-PtNi, being consistent with the conclusion of differential charge. However, H* of Heyrovsky or Tafel step is difficult to adsorb on Pt sites in (rich)NiO-PtNi due to the coverage of NiO layer. As shown in Fig. S16, by comparing the adsorption stability of OH_{ads} and H* on Pt, NiO-PtNi and NiO(rich)-PtNi, we found that H* prefers to be adsorbed on the surface of Pt species in PtNi and OH_{ads} prefers to be adsorbed on the surface of NiO. To further elucidate the structures related to the adsorption properties of NiO content, we measured the lengths of Pt-H and NiO-OH bonds around Pt and Ni atoms, as shown in Fig. 5d and e. Compared with PtNi and (rich)NiO-PtNi, NiO-PtNi has longer Pt-H and NiO-OH bonds, indicating that the separation sites in NiO-PtNi have strong OH* and H* desorption ability, thus achieving rapid alkaline hydrogen evolution kinetics. Obviously, despite producing a strong H* adsorption energy (Ni-H bond is only 1.46 A) in (rich) NiO-PtNi, the subsequent difficult desorption greatly hinders its hydrogen evolution rate due to H* forced adsorption of NiO surface in (rich)NiO-PtNi, resulting in poor catalytic activity.

Furthermore, we explored the reaction energy barriers of the

prepared catalysts for water splitting under alkaline conditions. As shown in Fig. 5f, we constructed the reaction path of alkaline HER, including the previous water dissociation to the formation of H* intermediates (Volmer step) and H_2 production (Tafel step or Heyrovsky step) [4,25,59]. NiO(rich)-PtNi shows the highest NiO-OH_{ads} energetics ($\Delta G_{H2O} = 1.7$ eV) and H* adsorption energy barrier ($\Delta G_{H^*} = 0.85$ eV) of all the samples, suggesting that the excessive NiO component covering the Pt sites in PtNi, H* has to be adsorbed on NiO, while the strong H* adsorption energy of NiO will hinder the hinder the generation of H_2, resulting in slow HER kinetics,which is consistent with the bond length results. In contrast, the separation sites in the NiO-PtNi heterostructure constructed with appropriate NiO content can accelerate the water dissociate step (Volmer step) and H* adsorption conversion (Tafel step or Heyrovsky step) simultaneously due to the strong adsorption capacity of NiO and adjacent Pt sites on water molecules and H*, respectively. As a result, the NiO-OH_{ads} energy on PtNi-NiO plummeted to only −0.08 eV, and the subsequent H* adsorption energy was also as low as −0.23 eV. In addition, the alkaline HER kinetics of pure PtNi is lower than PtNi-NiO, but higher than Pt (111), indicating the introduction of Ni to form PtNi alloy can increase the alkaline HER activity of Pt to a certain extent, due to electron transfer from Ni to Pt, and the narrow 3d state of Ni metal contributes to the coupling with water[28,60]. It is worth noting that the H* adsorption energy on the Pt (111) crystal surface is the lowest among all the catalysts, but the high Pt (111)-OH_{ads} energy leads to the its overall low reaction kinetics, which is consistent with the real performance of the Pt catalyst in the alkaline solution. In view of the above proven strong electron donating ability of ATO carriers can downshift the d-band centers of Ni and Pt atoms, achieving faster H_2O* and H* desorption. To provide a more comprehensive understanding, we further compared the adsorption energy analysis based on the two-step kinetic model. As clearly shown in Fig. 5h, suitable NiO component modification can accelerate both the Volmer-step and the Tafel-step, thereby achieving efficient alkaline HER catalytic activity. The above results indicate that the NiO-PtNi heterostructure constructed with appropriate NiO content can break the limit of Volmer step and significantly promote the adsorption and dissociation of water. In addition, the optimized NiO-PtNi dual site forms a optimized benign mechanism that balances H_2O*/H* adsorption and conversion, and synergistically improves the alkaline HER kinetics. As shown in Fig. 5g, we speculate the possible mechanism for enhanced HER activity the PtNi-NiO heterostructure in alkaline media: H_2O molecules first perform efficient adsorption-decomposition on NiO to form H* intermediates, promoting the Volmer step; then, exposed Pt site in PtNi acts as the H* adsorption center rapidly forms and converts H_2 through the Tafel step, thereby promoting alkaline HER performance.

4. Conclusions

In summary, we have successfully synthesized an ATO supported NiO-PtNi heterostructure catalyst with precise control of the NiO component at the interface by controlling the heat treatment temperature. The optimized NiO-PtNi/ATO catalyst achieves a low Tafel slope (only 25.5 mV dec^{-1}), a low overpotential (23.1 mV) at 10 mA·cm^{-2}, and an ultra-high mass activity of 8.4 A mg_{Pt}^{-1} at 70 mV, which exceeds most of the reported alkaline HER activity. Experiments and DFT analyses indicate ATO carrier optimizes the charge distribution of Pt and Ni atoms through strong electron-donating effects leading to a downshift of their d-band centers, thus optimizing the desorption of H2O* at the NiO site as well as H* at the Pt site in PtNi. In addition, the separation sites in the NiO-PtNi heterostructure constructed with appropriate NiO content can significantly reduce the water dissociation energy (Volmer step) and H* adsorption energy (Tafel step) simultaneously due to the strong desorption capacity of NiO and adjacent highly active Pt sites in PtNi on water molecules and H*, respectively. This exquisite NiO-PtNi heterostructure breaks the limit of Volmer step in the alkaline HER process and balances the absorption and desorption strength of the intermediate H_2O*/H*, thereby realizing rapid alkaline HER kinetics. Our work provides new insights into the construction of highly active catalysts through the precise design of heterogeneous interfaces.

CRediT authorship contribution statement

Yangyang Tan: Conceptualization, Methodology, Formal analysis, Investigation, Writing – original draft, Writing – review & editing. **Zeyi Zhang:** Carried out the theoretical calculations. **Wei Wu:** Carried out the theoretical calculations. **Suhao Chen:** Processed the figures. **Wei Chen:** Conceptualization, Methodology, Formal analysis. **Niancai Cheng:** Supervision, Formal analysis, Writing – original draft, Writing – review & editing, Visualization, Project administration.

Declaration of Competing Interest

The authors declare that they have no known competing financial interests or personal relationships that could have appeared to influence the work reported in this paper.

Data availability

Data will be made available on request.

Acknowledgements

This work was supported by the National Natural Science Foundation of China (grant no. 21875039); the Research Fund Program of Key Laboratory of Fuel Cell Technology of Guangdong Province; Project on the Integration of Industry-Education-Research of Fujian Province (2021H6020).

Appendix A. Supporting information

Supplementary data associated with this article can be found in the online version at doi:10.1016/j.apcatb.2023.122684.

References

[1] Z.Y. Yu, Y. Duan, X.Y. Feng, X. Yu, M.R. Gao, S.H. Yu, Clean and affordable hydrogen fuel from alkaline water splitting: past, recent progress, and future prospects, Adv. Mater. 33 (2021) 2007100, https://doi.org/10.1002/adma.202007100.

[2] L.-N. Zhang, R. Li, H.-Y. Zang, H.-Q. Tan, Z.-H. Kang, Y.-H. Wang, Y.-G. Li, Advanced hydrogen evolution electrocatalysts promising sustainable hydrogen and chlor-alkali co-production, Energy Environ. Sci. 14 (2021), 6191-62. 10.10.1039/d1ee02798k.

[3] N. Du, C. Roy, R. Peach, M. Turnbull, S. Thiele, C. Bock, Anion-exchange membrane water electrolyzers, Chem. Rev. 122 (2022) 11830–11895, https://doi.org/10.1021/acs.chemrev.1c00854.

[4] M. Zhou, H. Li, A. Long, B. Zhou, F. Lu, F. Zhang, F. Zhan, Z. Zhang, W. Xie, X. Zeng, D. Yi, X. Wang, Modulating 3d orbitals of Ni atoms on Ni-Pt edge sites enables highly-efficient alkaline hydrogen evolution, Adv. Energy Mater. 11 (2021) 2101789, https://doi.org/10.1002/aenm.202101789.

[5] Y. Li, C.K. Peng, H. Hu, S.Y. Chen, J.H. Choi, Y.G. Lin, J.M. Lee, Interstitial boron-triggered electron-deficient Os aerogels for enhanced pH-universal hydrogen evolution, Nat. Commun. 13 (2022) 1143, https://doi.org/10.1038/s41467-022-28805-8.

[6] J. Wu, J. Fan, X. Zhao, Y. Wang, D. Wang, H. Liu, L. Gu, Q. Zhang, L. Zheng, D. J. Singh, X. Cui, W. Zheng, Atomically Dispersed MoOx on Rhodium Metallene Boosts Electrocatalyzed Alkaline Hydrogen Evolution, Angew. Chem. Int Ed. Engl. 61 (2022) 202207512, https://doi.org/10.1002/anie.202207512.

[7] Y. Tan, R. Xie, S. Zhao, X. Lu, L. Liu, F. Zhao, C. Li, H. Jiang, G. Chai, D.J.L. Brett, P. R. Shearing, G. He, I.P. Parkin, Facile fabrication of robust hydrogen evolution electrodes under high current densities via Pt@Cu interactions, Adv. Funct. Mater. 31 (2021) 2105579, https://doi.org/10.1002/adfm.202105579.

[8] W.-X.L. Sulei Hu, Sabatier principle of metal-support interaction for design of ultrastable metal nanocatalysts, Science 374 (2021) 1360–1365, https://doi.org/10.1126/science.abi9828.

[9] J. Huang, L. Sementa, Z. Liu, G. Barcaro, M. Feng, E. Liu, L. Jiao, M. Xu, D. Leshchev, S.-J. Lee, M. Li, C. Wan, E. Zhu, Y. Liu, B. Peng, X. Duan, W. A. Goddard, A. Fortunelli, Q. Jia, Y. Huang, Experimental Sabatier plot for predictive design of active and stable Pt-alloy oxygen reduction reaction catalysts, Nat. Catal. 5 (2022) 513–523, https://doi.org/10.1038/s41929-022-00797-0.

[10] W. Sheng, Z. Zhuang, M. Gao, J. Zheng, J.G. Chen, Y. Yan, Correlating hydrogen oxidation and evolution activity on platinum at different pH with measured hydrogen binding energy, Nat. Commun. 6 (2015) 5848, https://doi.org/10.1038/ncomms6848.
[11] S. Ye, F. Luo, Q. Zhang, P. Zhang, T. Xu, Q. Wang, D. He, L. Guo, Y. Zhang, C. He, X. Ouyang, M. Gu, J. Liu, X. Sun, Highly stable single Pt atomic sites anchored on aniline-stacked graphene for hydrogen evolution reaction, Energy Environ. Sci. 12 (2019) 1000–1007, https://doi.org/10.1039/c8ee02888e.
[12] Z. Pu, T. Liu, G. Zhang, Z. Chen, D.S. Li, N. Chen, W. Chen, Z. Chen, S. Sun, General synthesis of transition-metal-based carbon-group intermetallic catalysts for efficient electrocatalytic hydrogen evolution in wide pH range, Adv. Energy Mater. 12 (2022) 2200293, https://doi.org/10.1002/aenm.202200293.
[13] Y. Yan, R. Zhang, Y. Yu, Z. Sun, R. Che, B. Wei, A.P. LaGrow, Z. Wang, W. Zhou, Interfacial optimization of PtNi octahedrons@Ti3C2MXene with enhanced alkaline hydrogen evolution activity and stability, Appl. Catal. B 291 (2021), 120100, https://doi.org/10.1016/j.apcatb.2021.120100.
[14] J. Luo, J. Wang, Y. Guo, J. Zhu, H. Jin, Z. Zhang, D. Zhang, Y. Niu, S. Hou, J. Du, D. He, Y. Xiong, L. Chen, S. Mu, Y. Huang, Metal-organic frameworks derived RuP2 with yolk-shell structure and efficient performance for hydrogen evolution reaction in both acidic and alkaline media, Appl. Catal. B 305 (2022), 121043, https://doi.org/10.1016/j.apcatb.2021.121043.
[15] X. Zhang, M. Zhang, Y. Deng, M. Xu, L. Artiglia, W. Wen, R. Gao, B. Chen, S. Yao, X. Zhang, M. Peng, J. Yan, A. Li, Z. Jiang, X. Gao, S. Cao, C. Yang, A.J. Kropf, J. Shi, J. Xie, M. Bi, J.A. van Bokhoven, Y.W. Li, X. Wen, M. Flytzani-Stephanopoulos, C. Shi, W. Zhou, D. Ma, A stable low-temperature H2-production catalyst by crowding Pt on alpha-MoC, Nature 589 (2021) 396–401, https://doi.org/10.1038/s41586-020-03130-6.
[16] K.L. Zhou, Z. Wang, C.B. Han, X. Ke, C. Wang, Y. Jin, Q. Zhang, J. Liu, H. Wang, H. Yan, Platinum single-atom catalyst coupled with transition metal/metal oxide heterostructure for accelerating alkaline hydrogen evolution reaction, Nat. Commun. 12 (2021) 3783, https://doi.org/10.1038/s41467-021-24079-8.
[17] Y.R. Hong, S. Dutta, S.W. Jang, O.F. Ngome Okello, H. Im, S.Y. Choi, J.W. Han, I. S. Lee, Crystal facet-manipulated 2D Pt nanodendrites to achieve an intimate heterointerface for hydrogen evolution reactions, J. Am. Chem. Soc. 144 (2022) 9033–9043, https://doi.org/10.1021/jacs.2c01589.
[18] A. Mosallanezhad, C. Wei, P. Ahmadian Koudakan, Y. Fang, S. Niu, Z. Bian, B. Liu, T. Huang, H. Pan, G. Wang, Interfacial synergies between single-atomic Pt and CoS for enhancing hydrogen evolution reaction catalysis, Appl. Catal. B 315 (2022), 121534, https://doi.org/10.1016/j.apcatb.2022.121534.
[19] Z. Lu, J. Xie, J. Hu, K. Wang, Y. Cao, In situ replacement synthesis of Co@NCNT encapsulated CoPt3 @Co2 P heterojunction boosting methanol oxidation and hydrogen evolution, Small 17 (2021) 2104656, https://doi.org/10.1002/smll.202104656.
[20] T. Xiong, X. Yao, Z. Zhu, R. Xiao, Y.W. Hu, Y. Huang, S. Zhang, M.J.T. Balogun, In situ grown Co-based interstitial compounds: non-3d metal and non-metal dual modulation boosts alkaline and acidic hydrogen electrocatalysis, Small 18 (2022), e2105331, https://doi.org/10.1002/smll.202105331.
[21] T. Xiong, B. Huang, J. Wei, X. Yao, R. Xiao, Z. Zhu, F. Yang, Y. Huang, H. Yang, M. S. Balogun, Unveiling the promotion of accelerated water dissociation kinetics on the hydrogen evolution catalysis of NiMoO4 nanorods, J. Energy Chem. 67 (2022) 805–813, https://doi.org/10.1016/j.jechem.2021.11.025.
[22] Y. Wang, L. Chen, X. Yu, Y. Wang, G. Zheng, Superb alkaline hydrogen evolution and simultaneous electricity generation by Pt-decorated Ni3N nanosheets, Adv. Energy Mater. 7 (2017) 1601390, https://doi.org/10.1002/aenm.201601390.
[23] S. Lu, Z. Zhuang, Investigating the influences of the adsorbed species on catalytic activity for hydrogen oxidation reaction in alkaline electrolyte, J. Am. Chem. Soc. 139 (2017) 5156–5163, https://doi.org/10.1021/jacs.7b00765.
[24] P. Wang, Q. Shao, J. Guo, L. Bu, X. Huang, Promoting alkaline hydrogen evolution catalysis on P-decorated, Ni-segregated Pt–Ni–P nanowires via a synergetic cascade route, Chem. Mater. 32 (2020) 3144–3149, https://doi.org/10.1021/acs.chemmater.0c00172.
[25] C. Zhang, X. Liang, R. Xu, C. Dai, B. Wu, G. Yu, B. Chen, X. Wang, N. Liu, H2 in situ inducing strategy on Pt surface segregation over low Pt doped PtNi5 nanoalloy with superhigh alkaline HER activity, Adv. Funct. Mater. 31 (2021) 2008298, https://doi.org/10.1002/adfm.202008298.
[26] N. Zhang, Q. Shao, X. Xiao, X. Huang, Advanced catalysts derived from composition-segregated platinum–nickel nanostructures: new opportunities and challenges, Adv. Funct. Mater. 29 (2019) 1808161, https://doi.org/10.1002/adfm.201808161.
[27] P. Wang, X. Zhang, J. Zhang, S. Wan, S. Guo, G. Lu, J. Yao, X. Huang, Precise tuning in platinum-nickel/nickel sulfide interface nanowires for synergistic hydrogen evolution catalysis, Nat. Commun. 8 (2017) 14580, https://doi.org/10.1038/ncomms14580.
[28] Z. Zhao, H. Liu, W. Gao, W. Xue, Z. Liu, J. Huang, X. Pan, Y. Huang, Surface-engineered PtNi-O nanostructure with record-high performance for electrocatalytic hydrogen evolution reaction, J. Am. Chem. Soc. 140 (2018) 9046–9050, https://doi.org/10.1021/jacs.8b04770.
[29] K. Lee, I. Park, Y. Cho, D. Jung, N. Jung, H. Park, Y. Sung, Electrocatalytic activity and stability of Pt supported on Sb-doped SnO2 nanoparticles for direct alcohol fuel cells, J. Catal. 258 (2008) 143–152, https://doi.org/10.1016/j.jcat.2008.06.007.
[30] J. Kim, H.-E. Kim, H. Lee, Single-atom catalysts of precious metals for electrochemical reactions, ChemSusChem 11 (2018) 104–113, https://doi.org/10.1002/cssc.201701306.
[31] J. Kim, C.-W. Roh, S.K. Sahoo, S. Yang, J. Bae, J.W. Han, H. Lee, Highly durable platinum single-atom alloy catalyst for electrochemical reactions, Adv. Energy Mater. 8 (2018), https://doi.org/10.1002/aenm.201701476.
[32] W. Chen, Z. Lei, T. Zeng, L. Wang, N. Cheng, Y. Tan, S. Mu, Structurally ordered PtSn intermetallic nanoparticles supported on ATO for efficient methanol oxidation reaction, Nanoscale 11 (2019) 19895–19902, https://doi.org/10.1039/c9nr07245d.
[33] F. Li, G.F. Han, H.J. Noh, J.P. Jeon, I. Ahmad, S. Chen, C. Yang, Y. Bu, Z. Fu, Y. Lu, J.B. Baek, Balancing hydrogen adsorption/desorption by orbital modulation for efficient hydrogen evolution catalysis, Nat. Commun. 10 (2019) 4060, https://doi.org/10.1038/s41467-019-12012-z.
[34] J.K. Norskov, F. Abild-Pedersen, F. Studt, T. Bligaard, Density functional theory in surface chemistry and catalysis, PNAS 108 (2011) 937–943, https://doi.org/10.1073/pnas.1006652108.
[35] M.T. Greiner, T.E. Jones, S. Beeg, L. Zwiener, M. Scherzer, F. Girgsdies, S. Piccinin, M. Armbruster, A. Knop-Gericke, R. Schlogl, Free-atom-like d states in single-atom alloy catalysts, Nat. Chem. 10 (2018) 1008–1015, https://doi.org/10.1038/s41557-018-0125-5.
[36] Y. Xie, J. Cai, Y. Wu, Y. Zang, X. Zheng, J. Ye, P. Cui, S. Niu, Y. Liu, J. Zhu, X. Liu, G. Wang, Y. Qian, Boosting water dissociation kinetics on Pt-Ni nanowires by N-induced orbital tuning, Adv. Mater. 31 (2019) 1807780, https://doi.org/10.1002/adma.201807780.
[37] Y. Yan, J. Lin, T. Xu, B. Liu, K. Huang, L. Qiao, S. Liu, J. Cao, S.C. Jun, Y. Yamauchi, J. Qi, Atomic-Level Platinum Filling into Ni-Vacancies of Dual-Deficient NiO for Boosting Electrocatalytic Hydrogen Evolution, Adv. Energy Mater. 12 (2022), https://doi.org/10.1002/aenm.202200434.
[38] T. Kou, M. Chen, F. Wu, T.J. Smart, S. Wang, Y. Wu, Y. Zhang, S. Li, S. Lall, Z. Zhang, Y.S. Liu, J. Guo, G. Wang, Y. Ping, Y. Li, Carbon doping switching on the hydrogen adsorption activity of NiO for hydrogen evolution reaction, Nat. Commun. 11 (2020) 590, https://doi.org/10.1038/s41467-020-14462-2.
[39] A. Nairan, C. Liang, S.-W. Chiang, Y. Wu, P. Zou, U. Khan, W. Liu, F. Kang, S. Guo, J. Wu, C. Yang, Proton selective adsorption on Pt–Ni nano-thorn array electrodes for superior hydrogen evolution activity, Energy Environ. Sci. 14 (2021) 1594–1601, https://doi.org/10.1039/d1ee00106j.
[40] Z. Chen, Y. Song, J. Cai, X. Zheng, D. Han, Y. Wu, Y. Zang, S. Niu, Y. Liu, J. Zhu, X. Liu, G. Wang, Tailoring the d-band centers enables Co4 N nanosheets to be highly active for hydrogen evolution catalysis, Angew. Chem. Int Ed. Engl. 57 (2018) 5076–5080, https://doi.org/10.1002/anie.201801834.
[41] M. Liu, J.A. Wang, W. Klysubun, G.G. Wang, S. Sattayaporn, F. Li, Y.W. Cai, F. Zhang, J. Yu, Y. Yang, Interfacial electronic structure engineering on molybdenum sulfide for robust dual-pH hydrogen evolution, Nat. Commun. 12 (2021) 5260, https://doi.org/10.1038/s41467-021-25647-8.
[42] J. Ding, L. Bu, S. Guo, Z. Zhao, E. Zhu, Y. Huang, X. Huang, Morphology and phase controlled construction of Pt-Ni nanostructures for efficient electrocatalysis, Nano Lett. 16 (2016) 2762–2767, https://doi.org/10.1021/acs.nanolett.6b00471.
[43] L. Zheng, X. Zhang, K.C. Bustillo, Y. Yao, L. Zhao, M. Zhu, W. Li, H. Zheng, Growth mechanism of core-shell PtNi-Ni nanoparticles using in situ transmission electron microscopy, Nanoscale 10 (2018) 11281–11286, https://doi.org/10.1039/c8nr01625a.
[44] S. Liu, Q. Zhang, Y. Li, M. Han, L. Gu, C. Nan, J. Bao, Z. Dai, Five-fold twinned Pd2NiAg nanocrystals with increased surface Ni site availability to improve oxygen reduction activity, J. Am. Chem. Soc. 137 (2015) 2820–2823, https://doi.org/10.1021/ja5129154.
[45] P. Wang, K. Jiang, G. Wang, J. Yao, X. Huang, Phase and Interface Engineering of Platinum-Nickel Nanowires for Efficient Electrochemical Hydrogen Evolution, Angew. Chem. Int Ed. Engl. 55 (2016) 12859–12863, https://doi.org/10.1002/anie.201606290.
[46] Z. Zhao, H. Liu, W. Gao, W. Xue, Z. Liu, J. Huang, X. Pan, Y. Huang, Surface-engineered PtNi-O nanostructure with record-high performance for electrocatalytic hydrogen evolution reaction, J. Am. Chem. Soc. 140 (2018) 9046–9050, https://doi.org/10.1021/jacs.8b04770.
[47] J. Kim, C.-W. Roh, S.K. Sahoo, S. Yang, J. Bae, J.W. Han, H. Lee, Highly durable platinum single-atom alloy catalyst for electrochemical reactions, Adv. Energy Mater. 8 (2018) 1701476, https://doi.org/10.1002/aenm.201701476.
[48] X. Jiang, H. Jang, S. Liu, Z. Li, M.G. Kim, C. Li, Q. Qin, X. Liu, J. Cho, The heterostructure of Ru2P/WO3/NPC synergistically promotes h2o dissociation for improved hydrogen evolution, Angew. Chem. Int Ed. Engl. 60 (2020) 4110–4116, https://doi.org/10.1002/anie.202014411.
[49] P. Wang, X. Zhang, J. Zhang, S. Wan, S. Guo, G. Lu, J. Yao, X. Huang, Precise tuning in platinum-nickel/nickel sulfide interface nanowires for synergistic hydrogen evolution catalysis, Nat. Commun. 8 (2017) 14580, https://doi.org/10.1038/ncomms14580.
[50] Y.L. Dang, T.L. Wu, H.Y. Tan, J.L. Wang, C. Cui, P. Kerns, W. Zhao, L. Posada, L. Y. Wen, S.L. Suib, Partially reduced Ru/RuO2 composites as efficient and pH-universal electrocatalysts for hydrogen evolution, Energy Environ. Sci. 14 (2021) 5433–5443, https://doi.org/10.1039/d1ee02380b.
[51] Q. Chen, B. Wei, Y. Wei, P. Zhai, W. Liu, X. Gu, Z. Yang, J. Zuo, R. Zhang, Y. Gong, Synergistic effect in ultrafine PtNiP nanowires for highly efficient electrochemical hydrogen evolution in alkaline electrolyte, Appl. Catal. B 301 (2022), 120754, https://doi.org/10.1016/j.apcatb.2021.120754.
[52] J. Huang, J. Han, T. Wu, K. Feng, T. Yao, X. Wang, S. Liu, J. Zhong, Z. Zhang, Y. Zhang, B. Song, Boosting hydrogen transfer during Volmer reaction at oxides/metal nanocomposites for efficient alkaline hydrogen evolution, ACS Energy Lett. 4 (2019) 3002–3030, 10.10.1021/acsenergylett.9b02359.
[53] J. Mahmood, F. Li, S.M. Jung, M.S. Okyay, I. Ahmad, S.J. Kim, N. Park, H.Y. Jeong, J.B. Baek, An efficient and pH-universal ruthenium-based catalyst for the hydrogen

evolution reaction, Nat. Nanotechnol. 12 (2017) 441–446, https://doi.org/10.1038/nnano.2016.304.
[54] T. Ma, H. Cao, S. Li, S. Cao, Z. Zhao, Z. Wu, R. Yan, C. Yang, Y. Wang, P.A. van Aken, L. Qiu, Y.G. Wang, C. Cheng, Crystalline lattice-confined atomic Pt in metal carbides to match electronic structures and hydrogen evolution behaviors of platinum, Adv. Mater. 34 (2022) 2206368, https://doi.org/10.1002/adma.202206368.
[55] P. Zhai, M. Xia, Y. Wu, G. Zhang, J. Gao, B. Zhang, S. Cao, Y. Zhang, Z. Li, Z. Fan, C. Wang, X. Zhang, J.T. Miller, L. Sun, J. Hou, Engineering single-atomic ruthenium catalytic sites on defective nickel-iron layered double hydroxide for overall water splitting, Nat. Commun. 12 (2021) 4587, https://doi.org/10.1038/s41467-021-24828-9.
[56] R. Xiao, P. Huang, T. Xiong, J. Wei, F. Wang, J. Deng, Z. Wang, M.S. Balogun, Advanced trifunctional electrodes for 1.5 V-based self-powered aqueous electrochemical energy devices, J. Mater. Chem. A 11 (2023) 374–384, https://doi.org/10.1039/d2ta05872c.
[57] Y. Tan, Z. Zhang, Z. Lei, L. Yu, W. Wu, Z. Wang, N. Cheng, Electronic modulation optimizes OH* intermediate adsorption on Co-Nx-C sites via coupling CoNi alloy in hollow carbon nanopolyhedron toward efficient reversible oxygen electrocatalysis, Appl. Catal. B (2021), https://doi.org/10.1016/j.apcatb.2021.121006.
[58] Y. Tang, F. Liu, W. Liu, S. Mo, X. Li, D. Yang, Y. Liu, S.-J. Bao, Multifunctional carbon-armored Ni electrocatalyst for hydrogen evolution under high current density in alkaline electrolyte solution, Appl. Catal. B 321 (2023), 122081, https://doi.org/10.1016/j.apcatb.2022.122081.
[59] C. Tsounis, B. Subhash, P.V. Kumar, N.M. Bedford, Y. Zhao, J. Shenoy, Z. Ma, D. Zhang, C.Y. Toe, S. Cheong, R.D. Tilley, X. Lu, L. Dai, Z. Han, R. Amal, Pt single atom electrocatalysts at graphene edges for efficient alkaline hydrogen evolution, Adv. Funct. Mater. 32 (2022) 2203067, https://doi.org/10.1002/adfm.202203067.
[60] H. Yin, S. Zhao, K. Zhao, A. Muqsit, H. Tang, L. Chang, H. Zhao, Y. Gao, Z. Tang, Ultrathin platinum nanowires grown on single-layered nickel hydroxide with high hydrogen evolution activity, Nat. Commun. 6 (2015) 6430, https://doi.org/10.1038/ncomms7430.